Shear Aligning Properties of a Main-Chain Thermotropic Liquid Crystalline Polymer

Wei-Jun Zhou and Julia A. Kornfield*

Chemical Engineering, 210-41, California Institute of Technology, Pasadena, California 91125

Wesley R. Burghardt

Department of Chemical Engineering, Northwestern University, Evanston, Illinois 60208

Received October 27, 2000

ABSTRACT: We report the first direct, quantitative measurements of the shear aligning properties of a main-chain thermotropic liquid crystalline polymer (LCP). We find that a model thermotrope with alternating mesogen and spacer structure is of the shear aligning type throughout its nematic range. The director rotates uniformly in the shear flow toward the Leslie alignment angle as probed by in situ flow conoscopy. The Leslie alignment angle becomes progressively closer to the flow direction as temperature decreases, corresponding to a decrease of the tumbling parameter λ with increasing order parameter S. Our measurements of $\lambda(S)$ enable direct comparison with predictions from molecular models, which predict that shear alignment prevails in the limit of flexible nematic chains. This is in direct contrast to rodlike lyotropic LCPs for which director tumbling is the rule.

I. Introduction

The key to attaining high mechanical performance for liquid crystalline polymers (LCPs) lies in control of structural and orientational behavior during processing flows. The qualitative orientation response in shear flow is strongly dependent on whether an LCP is of flow-aligning or director tumbling type. Flow alignment occurs when two hydrodynamic torques on the director balance at a particular angle (the "Leslie angle") with respect to the flow direction. Director tumbling occurs when no such alignment angle exists, and hydrodynamic torques act to rotate the director indefinitely in the shear plane (i.e., the flow-velocity gradient plane). Shear flow promotes macroscopic orientation of aligning nematics, while shear flow of tumbling nematics is highly susceptible to flow instabilies[1,2] and generally leads to low macroscopic orientation and complex morphology.

Despite the extreme qualitative differences between flow aligning and director tumbling behavior, definitive classification of polymeric nematics is rare. This is mainly because fundamental viscoelastic properties can only be obtained from experiments on defect-free monodomain samples, which are difficult to obtain for polymeric nematics due to their high viscosity. Nevertheless, the classification of flow aligning vs tumbling has been successfully carried out on two lyotropic solutions of rodlike polymers, both of which showed tumbling behavior,[3,4] in agreement with predictions of the Doi model for rodlike LCPs.[5] This discovery has profoundly impacted our understanding of lyotropic LCP rheology. It is now firmly established that tumbling is directly responsible for many of their unusual rheological characteristics (e.g., negative steady-state values of the first normal stress difference, N_1) and strongly impacts the shear orientation behavior of lyotropic LCPs.[6,7]

Similar advances are lacking for thermotropes. The added molecular flexibility in most thermotropic LCPs may alter their shear aligning properties in a nontrivial manner. In contrast to the Doi model's prediction for tumbling, all molecular theories for semiflexible polymeric nematics predict shear aligning behavior when the chain is sufficiently flexible.[8−10] In the limit of infinite ratio of chain length L to persistence length q, i.e., $L/q \rightarrow \infty$, Semenov found that polymeric nematics are exclusively flow aligning for all values of the order parameter.[8] Similar predictions have also been made by the nematic dumbbell model[9] and the nematic Rouse model.[10] Unfortunately, it is largely unknown whether thermotropes are flow aligning or tumbling. There is accumulated indirect evidence from mechanical and orientational studies suggesting that thermotropes with alternating mesogen and spacer structure may be flow aligning;[11−14] however, only one qualitative monodomain experiment has been reported on a mesogen-spacer type thermotrope ($OQ_{OE}O$-10).[15] A transition from shear aligning behavior at high temperature (close to the isotropization point, T_{ni}) to tumbling behavior was observed as temperature approaches the nematic-to-smectic A transition (T_{nS_A}). The tumbling behavior near T_{nS_A} for $OQ_{OE}O$-10 is attributed to pretransitional fluctuations of the smectic phase and may not be general to other polymeric nematics.

Recently, our group has made significant progress toward understanding of the flow behavior of main-chain thermotropic LCPs, observing indirect evidence that a model mesogen-spacer type thermotrope (DHMS-7,9) is of the shear aligning type.[14] In this paper, we present direct, quantitative measurements of the director response in a monodomain of DHMS-7,9 to a variety of shear flows. In situ flow conoscopy has been employed to monitor the director orientation during shear.[3,4,15] Quantitative determination of the tumbling parameter λ as a function of molecular order parameter S for this LCP provides the first opportunity to directly test theoretical predictions of $\lambda(S)$ from available molecular models.

* To whom correspondence should be addressed E-mail: jak@cheme.caltech.edu.

10.1021/ma0018493 CCC: $20.00
Published on Web 04/26/2001

II. Experimental Section

The model thermotropic polymer used here is a random copolyether of dihydroxy-α-methyl stilbene (DHMS) mesogens coupled with two different lengths of alkyl spacers, 7- and 9-(CH_2), to suppress its melting point. This polymer is referred to as DHMS-7,9.[14,16] The synthesis and characterization of DHMS-7,9 have been described in a previous paper.[14] All of our monodomain experiments were performed on a polymer with polystyrene-equivalent M_w of 11 000 g/mol (actual $M_w \approx$ 12 400 g/mol as determined from multiangle light scattering[17]) and polydispersity of 2.1. The nematic phase of this polymer spans from 104 to 157 °C as determined by differential scanning calorimetry (Perkin-Elmer DSC 7) and high-resolution powder X-ray diffraction, yet some remnants of birefringent structures may persist up to 181 °C when observed under a hot-stage polarizing light microscope. This is attributed to the wide distribution of molecular weight. Since T_{ni} determined by DSC and powder X-ray diffraction reflects the sample's bulk properties, we will use $T_{ni} = 157$ °C as the nematic-to-isotropic transition point.

Experiments were conducted using a custom-made shear cell. The design of our flow cell was inspired by apparatus available in the literature,[18−20] with the added capability for magnetic alignment due to its small size (compatible with magnet bore size of 15 cm). The essential features of this device comprise a static quartz window which can be accurately positioned using three micrometers with respect to a window mounted onto a spring-loaded mechanical translation stage. The interference fringes of the empty cell are used to adjust the alignment of the two window surfaces, giving parallelism to within ±2.5 μm across ∼1 cm field of view. Each window is independently heated by a mica heater (Minco, Inc.) and controlled with temperature stability to ±0.2 °C (controller CN-76000, Omega Inc.). The temperature variation over the whole window is estimated to be within ±1 °C. The motion of the bottom window is controlled by a microstepping motor (ζ-6104, Compumotor, Inc.), with a limit of 10 strain units for samples of 500 μm gap thickness.

The shear cell is used for monodomain preparation and in situ conoscopy studies at elevated temperature. The sample is sandwiched between two optical windows bearing rubbed polyimide alignment layers (SE-150, Nissan Chemical, Inc.). The rubbing directions of alignment layers have been kept either along the flow direction or along the neutral direction. The gap thickness is set to 500 or 600 μm at the measurement temperature. This sample thickness enables an observation of approximately 8−10 orders of interference in conoscopy. After loading the sample at a desired temperature in the nematic phase, we placed the sample cell inside a strong magnetic field (∼7 T) to enhance bulk alignment. The magnetic field is oriented collinear to the rubbing direction. In the magnetic field, the polymer samples were first heated to the isotropic state and then slowly cooled (∼10 °C/h) to the nematic phase for annealing (typically 30−50 h) until a monodomain is achieved, as evidenced by formation of a conoscopic pattern. The shear cell was then transferred to a polarizing optical microscope. Conoscopic interference figures were observed using monochromatic light ($\lambda_0 = 633$ nm) and photographed for subsequent analysis.

III. Conoscopy and Data Analysis

Conoscopy provides a noninvasive interference technique to observe the optical anisotropy and orientation of minerals and crystals. Since a nematic monodomain is a uniaxial crystal with its director orientation equivalent to its optical axis, conoscopy has been widely used to probe the director orientation of nematics during shear flow[3,4,20−24] and to measure the refractive indices of LCPs.[25] A thorough treatment of conoscopy principles may be found in monographs;[26] our intent here is to briefly review some optical results relevant to our experiments and analysis.

The conoscopic interference figure is generated by passing a highly convergent cone of light through the sample placed between crossed polarizers. Light rays having different incident angle experience distinct optical path length differences between their ordinary and extraordinary rays, and the interference figures that result are imaged on the back focal plane of the objective lens. Visualization of the conoscopic interference figures is made possible by the use of a Bertrand lens. For an undistorted planar nematic monodomain, a typical conoscopy pattern consists of symmetric hyperbola-like principal isochromates placed parallel and perpendicular to the director orientation.

The conoscopic pattern may be used to extract the two refractive indices n_o and n_e, for the ordinary ray and extraordinary ray, respectively. When the plane of light incidence (containing light wave propagation vector **k** and electric field vector **E**) is parallel to the director **n**, the optical path difference, $\delta_{||}$, is given by[27]

$$\delta_{||}(\theta_i) = \frac{2\pi(\Delta n)d}{\lambda_0}\left(1 - \left(\frac{\sin\theta_i}{n_0}\right)^2\right)^{1/2} \quad (1)$$

where θ_i is the incident angle in the air, and Δn is the birefringence of the nematic. When the plane of light incidence is perpendicular to **n**, $\delta_\perp$ is given by[28]

$$\delta_\perp(\theta_i) \simeq \frac{2\pi(\Delta n)d}{\lambda_0}\left(1 - \left(\frac{\sin\theta_i}{n_{eff}}\right)^2\right)^{-1/2} \quad (2)$$

where n_{eff} is an effective refractive index of the equivalent isotropic medium, defined as

$$n_{eff} = \frac{n_e + 2n_o}{3} \quad (3)$$

The two refractive indices can be obtained by fitting eqs 1 and 2 to the positions of minima and maxima of transmitted light intensity on a conoscopic interference figure. It is noteworthy that $\delta_{||}$ decreases monotonically with increasing θ_i, whereas $\delta_\perp$ increases monotonically with increasing θ_i, so the symmetry center of the interference figure corresponds to the light path for which the sample retardance passes through a saddle point.

Upon application of shear flow, the director will rotate against the vorticity for a shear aligning nematic, but with the vorticity for a tumbling nematic. The rotation of the director results in a shift of the symmetry center of interference figure. The apparent rotation angle θ_{app} for which the light path corresponds to the symmetry center is given by

$$\sin\theta_{app} = \left(\frac{r}{R}\right)\frac{NA}{n_{eff}} \quad (4)$$

where r is the displacement of the symmetry center of the hyperbolic fringe pattern, R is the radius of the full field of view of the conoscopic pattern, and NA is the numerical aperture of the objective lens. It must be noted that θ_{app} is not equal to the actual rotation angle of the director θ. The general relationship between θ and θ_{app} has been given in the literature[27] and is quite complex. Nevertheless, in the limit of small birefringence, a rather simple relation can be derived, giving $\theta \simeq {}^1/_2\theta_{app}$. We find this approximation is good even at a

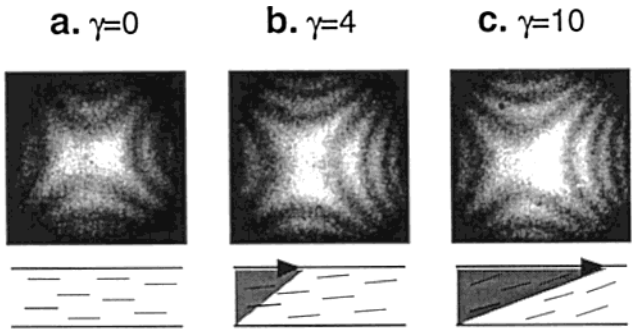

Figure 1. Conoscopic patterns observed in a planar DHMS-7,9 monodomain at 130 °C for (a) quiescent condition and shearing for (b) 4 strain units and (c) 10 strain units at a rate of 0.02 s^{-1}. The schematic diagrams below each conoscopic pattern illustrate the deformation geometry and direction of director rotation.

fairly large Δn; for example, when $\Delta n \simeq 0.2$, the error represented by this approximation is only about 4%.

IV. Results

Qualitative Determination of Shear Aligning vs Tumbling Character. Quiescent monodomains exhibit the hyperbolic fringe pattern characteristic of planar, optically uniaxial nematics (Figure 1a). Upon inception of shear flow, the interference figures are observed to shift in the direction that indicates the director rotates against the vorticity of the shear flow (Figure 1b,c). This observation provides unambiguous evidence that DHMS-7,9 is of shear aligning type. The same qualitative behavior was seen at all temperatures within the nematic phase.

Quantitative Determination of the Tumbling Parameter λ. The quantitative value of λ may be extracted from the strain dependence of the director rotation. Owing to the high viscosity of this polymer sample, the shear rates we have chosen (on the order of 10^{-2} s^{-1}) fall in the range of high Ericksen number $Er \gg 1$, where $Er = (\eta\dot{\gamma}d^2)/K$ (η and K are characteristic viscous and elastic constants), so distortional elastic effects are weak compared to viscous effects. In addition, the shear rate is small enough that the effect of conformational elasticity and changes in molecular order parameter can be neglected. In this range of $\dot{\gamma}$, the director experiences a uniform rotation in response to an applied shear flow, except within two thin orientational boundary layers near the anchoring surfaces.

When the response of the director remains in the flow-velocity gradient plane, the evolution of director orientation during flow can be described by the Leslie–Ericksen theory as follows:[29,30]

$$\frac{d\theta}{d\gamma} = \frac{\alpha_2 \sin^2\theta - \alpha_3 \cos^2\theta}{\alpha_3 - \alpha_2} \qquad (5)$$

where θ is the angle of the director orientation relative to the flow direction, γ is the applied shear strain, and α_2 and α_3 are two of the six Leslie–Ericksen viscosity coefficients. Thus, when hydrodynamic forces dominate over distortional elasticity, the director rotation is independent of shear rate and solely a function of applied strain. Indeed, no shear rate dependence of director rotation was observed in steady shear of a planar nematic monodomain (Figure 2). We have also imposed incremental stepwise shearing on a monodomain and found that the director response $\theta(\gamma)$ is essentially identical to that observed upon inception of steady shear (Figure 3). These results confirm that the hydrodynamic terms are dominant and, more importantly, that the basic analysis of Leslie–Ericksen theory applies to polymeric nematics at shear rates that are slow relative to molecular relaxation. Our rheological studies indicate that the relaxation time of a higher molecular weight DHMS-7,9 (M_w = 28 440 g/mol) is approximately $\tau \approx 3-4$ s,[14] and that of the present 11 000 g/mol DHMS-7,9 is much smaller. Therefore, the shear rates used in our experiments ($\dot{\gamma} \leq 0.05$ s^{-1}) are all low enough that chain conformation is not distorted ($\dot{\gamma}\tau \ll 0.1$).

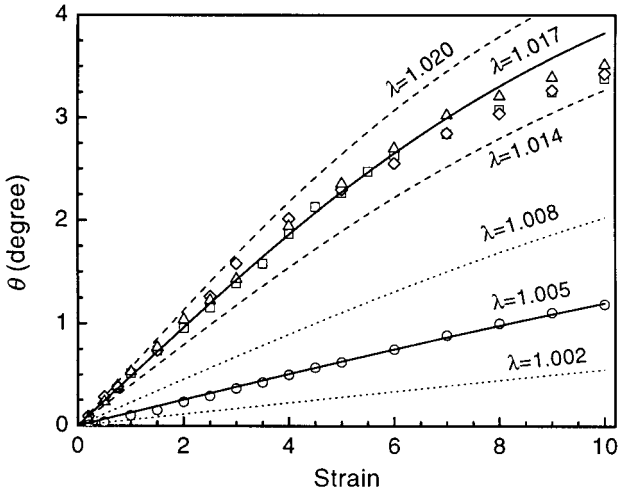

Figure 2. Director rotation θ as a function of applied strain in DHMS-7,9 monodomains. Data are presented for continuous shearing at 130 °C at shear rates of 0.01 [□], 0.02 [◇], and 0.05 s^{-1} [△] and at 110 °C at a shear rate of 0.02 s^{-1} [○]. The two solid lines are fits of eq 6 to $\theta(\gamma)$ at 130 and 110 °C using values of $\lambda = 1.017$ and 1.005, respectively. The dashed and dotted curves are computed at λ values differing by ±0.003 from the best fit values.

For a shear aligning nematic, eq 5 may be integrated to give

$$\tan\theta = \sqrt{\frac{\lambda - 1}{\lambda + 1}} \tanh\left(\frac{\gamma}{2}\sqrt{\lambda^2 - 1}\right) \qquad (6)$$

In this expression, $\lambda \equiv (\alpha_2 + \alpha_3)/(\alpha_2 - \alpha_3)$ is the tumbling parameter. Shear alignment corresponds to values $|\lambda| > 1$, and a steady orientation is obtained as $\gamma \rightarrow \infty$. The Leslie alignment angle increases with increasing λ. Quantitative values of λ can be accurately determined by fitting eq 6 to the director response $\theta(\gamma)$. For example, the director reorientation at 130 °C tracks the theoretical trajectory for director evolution with $\lambda = 1.017$, while $\theta(\gamma)$ at 110 °C accords with $\lambda = 1.005$ (solid lines in Figure 2). Curves for λ above and below these values by 0.003 are also shown for comparison, demonstrating the high precision with which λ may be determined using this technique.

Temperature Dependence of the Tumbling Parameter, $\lambda(T)$. With increasing temperature, λ increases: the director systematically rotates faster as a function of applied strain (Figures 2 and 3), approaching the Leslie alignment angle at lower applied strain, and the flow alignment angle becomes progressively farther from the flow direction. While the tumbling parameter of DHMS-7,9 decreases monotonically with decreasing temperature, it remains above unity throughout the

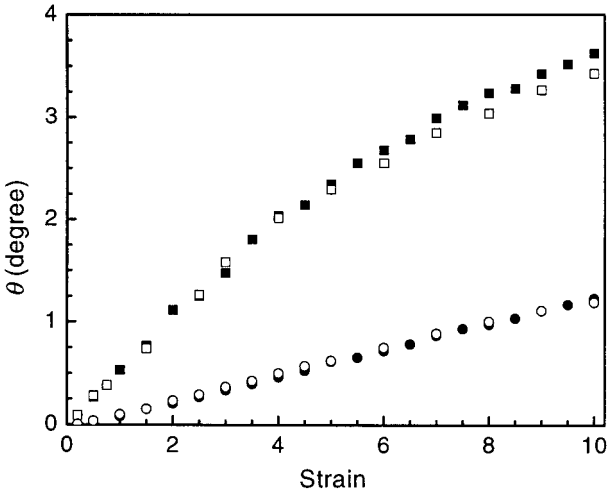

Figure 3. Director rotation θ as a function of applied strain during stepwise application of shear strain at temperatures of 130 °C (filled square) and 110 °C (filled circle) in DHMS-7,9. Data for continuous shearing at 0.02 s^{-1} (open symbols) are also included for comparison.

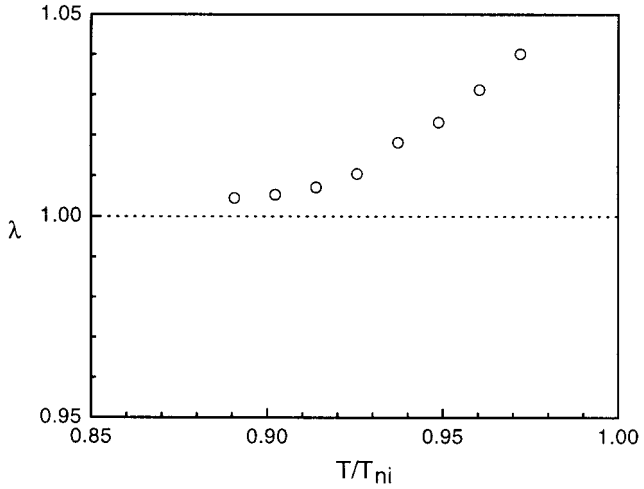

Figure 4. Tumbling parameter λ as a function of reduced temperature T/T_{ni}. The dotted line separates the shear aligning region ($|\lambda| > 1$) from the tumbling region ($|\lambda| < 1$).

nematic range (Figure 4). The observed temperature dependence of λ is qualitatively similar to that of small molecule liquid crystals, such as MBBA.[31] In the context of small molecule liquid crystals, the trend of λ with T is explained in terms of the increase in the order parameter S with deeper undercooling into the nematic phase.

Temperature Dependence of the Order Parameter, *S*(*T*). Since a direct comparison with molecular theories requires $\lambda(S)$, we estimate $S(T)$ using the observed temperature dependence of the optical anisotropy. Like the ordinary refractive index (n_o) of small molecule liquid crystals, n_o of DHMS-7,9 shows a very weak temperature dependence over the entire nematic range, whereas the extraordinary refractive index n_e decreases monotonically as the nematic-to-isotropic transition is approached. We find the refractive indices can be reasonably well described by the two-parameter equation of the Vuks model,[32,33] given by

$$\log[(n_e^2 - n_o^2)/(n^2 - 1)] = \alpha + \beta \log(1 - T/T_{ni}) \quad (7)$$

Here, $n^2 = (n_e^2 + 2n_o^2)/3$ represents a squared average

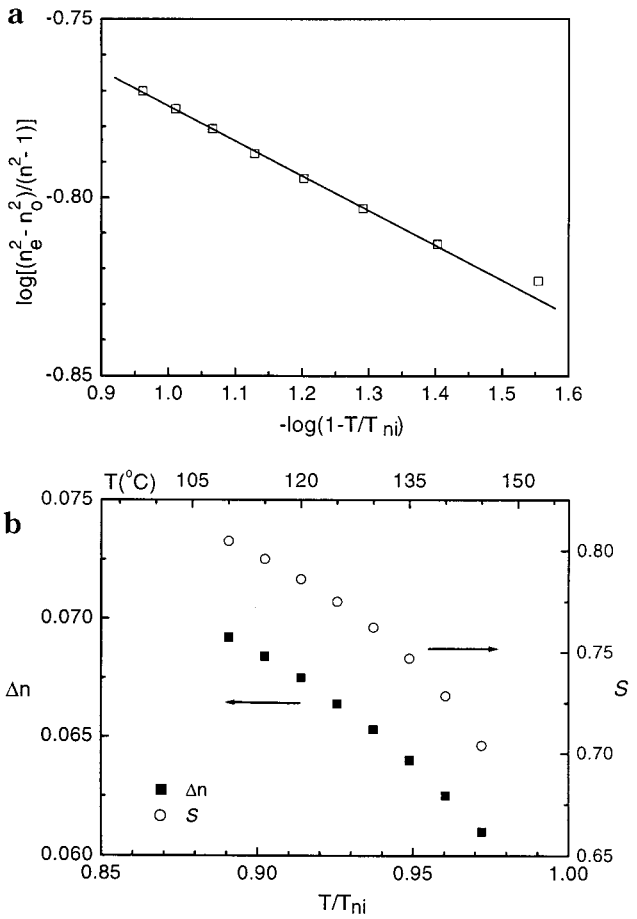

Figure 5. (a) Analysis of optical anisotropy of DHMS-7,9 using Vuks' model to extract the temperature dependence of the order parameter. (b) Birefringence (Δn) and order parameter (S) as functions of reduced temperature T/T_{ni}.

refractive index of the liquid crystal, and α is related to the anisotropy of its molecular polarizability. The parameter β describes the temperature dependence of the order parameter (S) by a simple relation

$$S = \left(1 - \frac{T}{T_{ni}}\right)^{\beta} \quad (8)$$

The internal consistency of the Vuks model has been proven in small molecule liquid crystals, and the same analysis seems also to be valid for the present polymeric liquid crystal DHMS-7,9 (Figure 5a). As is the case of small molecule LCs,[33] a slight deviation from the Vuks model is observed as the temperature approaches the nematic-to-isotropic transition. This curvature may be attributed to the pretransitional effect.[33]

With increasing temperature the order parameter and, consequently, birefringence decrease (Figure 5b). From the observed refractive indices, the order parameter of DHMS-7,9 is estimated to lie between 0.7 and 0.8 within the nematic range (Figure 5b). This value of S is larger than that of small molecule LCs at the same T/T_{ni}, probably due to stronger excluded-volume interaction in polymeric nematics. The shapes of $S(T/T_{ni})$ and $\Delta n(T/T_{ni})$ are very much alike, as expected. (In the limit of small Δn, the Vuks model gives Δn proportional to S.)

Relaxation Following Cessation of Shear Flow. The shear-induced director rotation relaxes following cessation of shear flow. The director orientation roughly

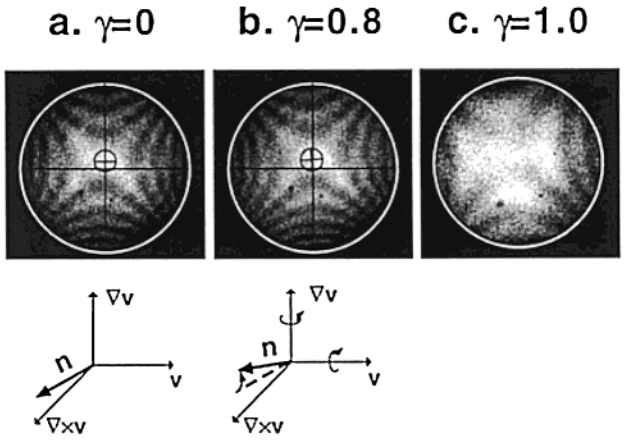

Figure 6. Director rotation of a planar DHMS-7,9 monodomain with its initial orientation along the vorticity direction for shearing at a rate of 0.02 s^{-1} at $T = 130$ °C. The schematic diagrams illustrate how the director rotates in response to the applied flow: the rotation of the director about the gradient direction is dominated by α_2, and the observed sense of rotation is indicative of $\alpha_2 < 0$; the rotation about the flow direction is dominated by α_3, and the observed sense of rotation is consistent with $\alpha_3 < 0$.[40,48]

follows an exponential decay with a characteristic decay time $\tau_d \approx 9$ h at 130 °C. This relaxation is much slower than that of small molecule nematics (~800 s at the present sample thickness).[22] Since the decay time scales as the ratio of the rotational viscosity γ_1 to characteristic elastic constants K_i, $\tau_d \propto \gamma_1/K_i$, the slow director relaxation of this LCP implies a large value for γ_1/K_i. Since the elastic constant of a mesogen-spacer type LCP has been reported to be only about 1 order of magnitude larger than for small molecule LCs,[34] the 2 orders of magnitude increase in γ_1/K_i for the present LCP compared to small molecule LCs is dominated by the change in γ_1 (approximately 360 Pa·s for 11 kg/mol DHMS-7,9[17] vs ~0.1 Pa·s for typical small molecule nematics[35]). This result further shows that the shear rates used in the present experiments are sufficient to overwhelm distortional elasticity ($Er = \dot{\gamma}\tau_d \approx 10^3$).

Shear Response with Director in Vorticity Direction. An initial director orientation along the vorticity direction is unstable to imposed shear for both tumbling and flow-aligning nematics; however, the nature of the instability is fundamentally different for the two cases. In the presence of distortional elastic effects, a "roll-cell" instability occurs in tumbling nematics (for $Er > 10^2$),[4,36−39] while just above the critical Er number ($Er_c \approx 10-10^2$), flow-aligning nematics rotate to a stable orientation intermediate between the vorticity direction and Leslie alignment angle at which hydrodynamic and elastic torques balance.[40−42]

Here, we examine the response of DHMS-7,9 to inception of shear in the region of very high $Er \geq 10^3$. To observe an initial coherent response, we adopt the usual procedure of imposing a small orientational bias (alignment layers are placed with their rubbing directions antiparallel, providing pretilt about the velocity direction of < 2°). During the first strain unit of shear, the director rotates in a manner consistent with $\alpha_2 < 0$ and $\alpha_3 < 0$ (Figure 6a,b). Roll cells are not observed even to an applied strain of $\gamma = 5$. Instead, the conoscopic figure fades for $\gamma \geq 1$ (Figure 6c), while the sample has a uniform appearance in orthoscopic observation.

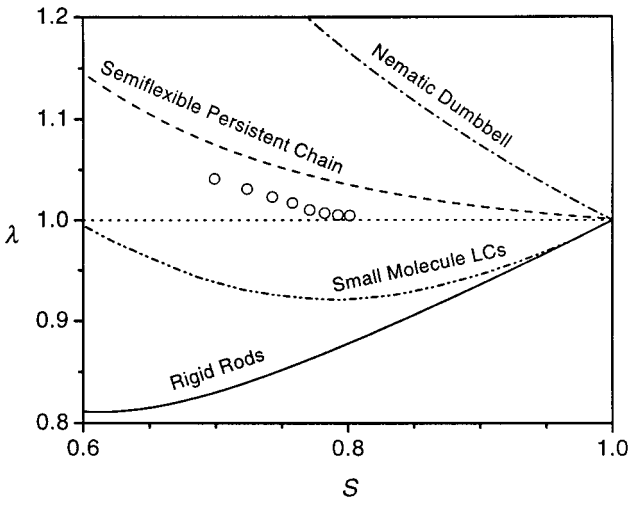

Figure 7. Tumbling parameter λ as a function of order parameter (S) for DHMS-7,9. The dot−dash curve [− · −] and dash curve [− − −] represent calculations of λ from the nematic dumbbell model and semiflexible nematic chain model at the limit of $L/q \rightarrow \infty$, respectively. The double-dot−dash curve [− ·· −] shows the predicted values of λ as a function of S for small molecule liquid crystals using a Maier−Saupe potential, and the solid curve [−] represents the predictions of λ from the Doi model of rigid rods.

V. Discussion

A Unifying View of the Aligning Properties of Mesogen-Spacer LCPs. The quantitative determination of λ in combination with mechanical and in situ shear orientation studies[14] in one model system provides a foundation for interpreting indirect evidence of shear aligning character for other mesogen-spacer type thermotropic LCPs. In steady shear, DHMS-7,9 exhibits high shear-induced orientation in the nematic phase that is nearly independent of shear rate, a signature of shear aligning behavior. Similar shear orientation behavior has been observed in a different mesogen-spacer type thermotropic LCP (PSHQ-6,12),[13] suggesting that it too is of shear aligning type. The flow aligning character of DHMS-7,9 and PSHQ-6,12 is also in accord with their similarities in transient shear rheology: neither DHMS-7,9 nor PSHQ-6,12 shows the multiple shear stress oscillations that are characteristic of tumbling nematics. Finally, the prior qualitative conoscopy study on yet another mesogen-spacer type LCP ($OQ_{OE}O$-10) showed that it is also shear aligning in the nematic phase away from its nematic-to-smectic phase transition.[15] Taken together, these are all evidence for shear aligning character of mesogen-spacer type LCPs. Thus, shear alignment may be dominant in mesogen-spacer type LCPs in general—at least when the chains are sufficiently long.

Comparison of $\lambda(S)$ with Small Molecule LCs. Like shear aligning small molecule LCs, the tumbling parameter of DHMS-7,9 decreases with increasing order parameter (Figure 7); however, in contrast to small molecule LCs that are predicted to cross over to tumbling type when S is above 0.6,[43] DHMS-7,9 remains shear aligning to $S = 0.8$. On the basis of molecular models, this discrepancy may be attributed to the effect of chain flexibility in mesogen-spacer type LCPs.

Comparisons of $\lambda(S)$ with Molecular Models. Two different theoretical approaches have been taken in the literature to account for the effect of chain flexibility on main chain LCP dynamics, and both predict shear-

aligning behavior at high flexibility,[8−10] in agreement with the data presented here for DHMS-7,9. The first approach explicitly incorporates molecular flexibility into model formulations, including the nematic dumbbell model[9] and nematic Rouse model.[10] These two models are essentially anisotropic generalizations of the ordinary dumbbell model and Rouse model, representing the LCP chain by nematic rods linked by elastic springs. According to the nematic dumbbell model, flow alignment occurs at all values of the molecular order parameter, and λ depends on S according to

$$\lambda = \frac{2 + S}{3S} \tag{9}$$

The nematic dumbbell model captures the qualitative trend of λ decreasing as a function of S, but it substantially overpredicts the value of λ (Figure 7). Quantitative comparisons between the nematic Rouse model and experimental data are not given, since λ is not explicitly expressed as a function of the order parameter. Nevertheless, the shear aligning character of flexible LCPs is also captured by the nematic Rouse model.

The second approach extends the Doi model to semiflexible chains. Although a general theory for the effect of molecular flexibility on λ is still lacking, the limits of slight and infinite flexibility have been examined. For slightly flexible rods, i.e., a small but finite ratio of chain length L to persistence length q ($0 < L/q \ll 1$), Subbotin found that λ is less than predicted for perfectly rigid rods ($L/q = 0$) except at high order parameters ($S > 0.82$),[44] suggesting that slightly flexible rods are more prone to be tumbling than are rigid rods. On the other hand, for highly flexible nematic chains, $L/q \rightarrow \infty$, Semenov found λ is always above unity.[8] Therefore, flexible polymeric nematics are predicted to be flow aligning for all values of the order parameter. This prediction reinforces the qualitative character predicted by the nematic dumbbell model and quantitatively shows much better accord with $\lambda(S)$ observed for DHMS-7,9 (Figure 7). Further, Semenov asserts that for finite L/q the values of $\lambda(S)$ fall below the upper bound established for $L/q \rightarrow \infty$.[8] This would further improve the agreement with the present results, since DHMS-7,9 of 11 000 g/mol molecular weight only has a modest L/q. (Based on independent measurement of the molecular weight dependence of viscous coefficients, a DHMS-7,9 chain of this length is estimated to form only $O(1)$ hairpins.[17]) Thus, combining our results with Subbotin and Semenov's theoretical predictions, it seems that a critical L/q value might exist, below which a transition from flow alignment to tumbling occurs at high order parameter but above which flow alignment occurs for all values of S in the nematic phase.

Physical Insights on the Effect of Flexibility. We find that Semenov's semiflexible nematic chain model best describes the dynamical behavior of flexible LCPs. However, the physical basis for the prediction of shear aligning behavior in Semenov's model is not stated. For mesogen-spacer type thermotropes, the chain flexibility is so high that mesogens along a given chain can have different orientations, as illustrated in Figure 8. These mesogens will experience different hydrodynamic torques; however, connectivity through the chain limits their ability to rotate at different rates. This combination of the variation of the hydrodynamic torques with position along the chain and the effect of chain connectivity is captured by Semenov's governing equations. The resulting frustration appears to be responsible for suppressing tumbling motion.

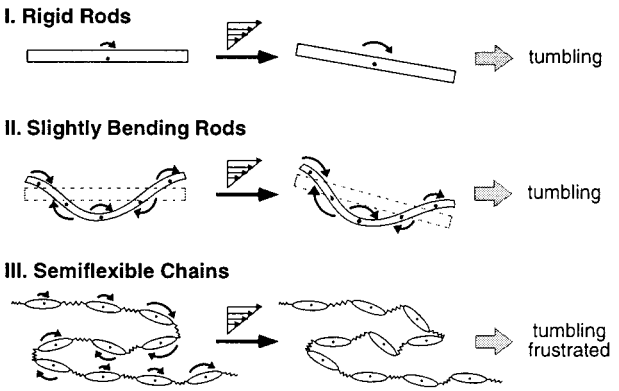

Figure 8. Schematic illustration of the nonmonotonic effect of molecular flexibility on the aligning properties of main-chain LCPs. Curved arrows represent hydrodynamic torque exerted locally on the polymer; its length indicates the magnitude of local torque. (I) Rigid rods: net hydrodynamic torques always act to rotate the director, leading to director tumbling. (II) Slightly bending rods are subject to even larger hydrodynamic torques than rigid rods and consequently are even more susceptible to tumbling motion. (III) Semiflexible chains: mesogens along the same chain have different orientation, so they experience different torques; however, chain connectivity frustrates their ability to rotate at different rates, suppressing tumbling motion.

This physical picture may not generalize to the situation where the nematic chain has little flexibility, such as commercial thermotropes Vectra and Xydar. For these materials, the nematic chain has no flexible spacers, only units that introduce chain kinks. Since its persistence length can be fairly long, the orientation of mesogens only meanders slightly along the chain contour: it is much harder to envision formation of hairpins under these circumstances. During shear, hydrodynamic torques would rotate the entire chain (Figure 8), so tumbling would still exist in this type of LCP, as predicted for slightly flexible rods[44,45] and for the directed-chain limit of the nematic Rouse model.[10] Indeed, thermotropic hydroxypropylcellulose (HPC) has been inferred to exhibit tumbling behavior from an extrapolation of a series of mechanical experiments on tumbling lyotropic HPC solutions to a concentration of 100%.[46] The hypothesis of tumbling in HPC is also consistent with recent orientation studies showing that shear is only able to induce a low degree of orientation at small shear rate.[47] Interestingly, however, the absolute flexibility of HPC, expressed as the ratio of persistence length to chain diameter, might not be that dissimilar from some main-chain thermotropes with flexible spacers [see caption to Figure 11.2 of ref 34]. This suggests the possibility that the *concentration* of flexibility into the hydrocarbon spacer, facilitating formation of hairpin conformations in the nematic melt, might be the essential characteristic of the mesogen-spacer-type polymers that results in flow-aligning dynamics.

VI. Conclusion

Quantitative determination of $\lambda(T)$ for mesogen-spacer type thermotropic LCP, together with estimation of its temperature-dependent order parameter $S(T)$, shows that (1) this model LCP is flow aligning throughout its nematic range, (2) the rheological and orientational behavior of this model polymer can be definitively

attributed to flow-aligning character, providing the basis for assigning the character of other thermotropic LCPs based on more widely available rheological and orientational measurements, and (3) molecular models of main-chain LCPs that incorporate chain flexibility successfully capture the qualitative and even semiquantitative character of $\lambda(S)$, while models for rigid-rod LCPs and small-molecule LCs do not. The importance of chain flexibility may provide a useful molecular design principle for commercial thermotropes: by incorporating units that increase chain flexibility, it may be possible to convert LCPs that exhibit tumbling behavior into LCPs with flow-aligning character. In turn, the change in flow character may facilitate production of materials with uniform, high degrees of molecular orientation.

Acknowledgment. Financial support was provided by the Air Force Office of Scientific Research Liquid Crystal-MURI (Grant F49620-97). We thank Prof. Peter Palffy-Muhoray of Kent State University for assistance with liquid crystal alignment.

References and Notes

(1) Pieranski, P.; Guyon, E. *Phys. Rev. Lett.* **1974**, *32*, 924.
(2) Cladis, P. E.; Torza, S. *Phys. Rev. Lett.* **1975**, *35*, 1283.
(3) Burghardt, W. R.; Fuller, G. G. *Macromolecules* **1991**, *24*, 2546.
(4) Srinivasarao, M.; Berry, G. C. *J. Rheol.* **1991**, *35*, 379.
(5) Kuzuu, N.; Doi, M. *Jpn. J. Phys. Soc.* **1984**, *53*, 1031.
(6) Marrucci, G.; Greco, F. *Adv. Chem. Phys.* **1993**, *LXXXVI*, 331.
(7) Burghardt, W. R. *Macromol. Chem. Phys.* **1998**, *199*, 471.
(8) Semenov, A. N. *Sov. Phys. JETP* **1987**, *66*, 712.
(9) Maffettone, P. L.; Marrucci, G. *J. Rheol.* **1992**, *36*, 1547.
(10) Long, D.; Morse, D. C. *Europhys. Lett.* **2000**, *49*, 255.
(11) Cocchini, F.; Nobile, M. R.; Acierno, D. *J. Rheol.* **1991**, *35*, 1171.
(12) Chang, S.; Han, C. D. *Macromolecules* **1997**, *30*, 1656.
(13) Ugaz, V. M.; Burghardt, W. R. *Macromolecules* **1998**, *31*, 8474.
(14) Zhou, W.-J.; Kornfield, J. A.; Ugaz, V. M.; Burghardt, W. R.; Link, D. R.; Clark, N. A. *Macromolecules* **1999**, *32*, 5581.
(15) Srinivasarao, M.; Garay, R. O.; Winter, H. H.; Stein, R. S. *Mol. Cryst. Liq. Cryst.* **1992**, *223*, 29.
(16) Hall, E.; Ober, C. K.; Kramer, E. J.; Colby, R. H.; Gillmor, J. R. *Macromolecules* **1993**, *26*, 3764.
(17) Zhou, W.-J.; Kornfield, J. A.; Burghardt, W. R. Manuscript in preparation.
(18) Alderman, N. J.; Mackley, M. R. *Faraday Discuss. Chem. Soc.* **1985**, *79*, 149.
(19) Larson, R. G.; Mead, D. W. *Liq. Cryst.* **1992**, *12*, 751.
(20) Mather, P. T.; Pearson, D. S.; Burghardt, W. R. *J. Rheol.* **1995**, *39*, 627.
(21) Wahl, J.; Fischer, F. *Opt. Commun.* **1972**, *5*, 341.
(22) Müller, J. A.; Stein, R. S.; Winter, H. H. *Rheol. Acta* **1994**, *33*, 473.
(23) Ternet, D. J.; Larson, R. G.; Leal, L. G. *Rheol. Acta* **1999**, *38*, 183.
(24) Boudreau, D. M.; Winter, H. H.; Lillya, C. P.; Stein, R. S. *Rheol. Acta* **1999**, *38*, 503.
(25) Mattoussi, H.; Srinivasarao, M.; Kaatz, P. G.; Berry, G. C. *Macromolecules* **1992,** *25*, 2860.
(26) Bloss, F. D. *An Introduction to the Methods of Optical Crystallography*; Holt, Rinehart and Winston: New York, 1961.
(27) Scheffer, T. J.; Nehring, J. *J. Appl. Phys.* **1977**, *48*, 1783.
(28) Born, M.; Wolf, E. *Principles of Optics*, 7th ed.; Cambridge University Press: New York, 1999.
(29) Ericksen, J. L. *Arch. Rat. Mech. Anal.* **1960**, *4*, 231.
(30) Leslie, F. M. *Arch. Rat. Mech. Anal.* **1968**, *28*, 265.
(31) Kneppe, H.; Schneider, F.; Sharma, N. K. *J. Chem. Phys.* **1982**, *77*, 3203.
(32) Vuks, M. F. *Opt. Spectrosc.* **1966**, *20*, 644.
(33) Haller, I. *Prog. Solid State Chem.* **1975**, *10*, 103.
(34) Larson, R. G. *The Structure and Rheology of Complex Fluids*; Oxford University Press: Oxford, 1999.
(35) Larson, R. G. *Constitutive Equations for Polymer Melts and Solutions*; Butterworths: Markham, 1988.
(36) Larson, R. G. *J. Rheol.* **1993**, *37*, 175.
(37) Guyon, E.; Janossy, I.; Pieranski, P.; Jonathan, J. M. *J. Opt. (Paris)* **1977**, *8*, 357.
(38) Dubois-Violette, E.; Durand, G.; Guyon, E.; Manneville, P.; Pieranski, P. *Solid State Phys. (Suppl.)* **1978**, *14*, 147.
(39) Mather, P. T.; Pearson, D. S.; Larson, R. G. *Liq. Cryst.* **1996**, *20*, 539.
(40) Pieranski, P.; Guyon, E. *Solid State Commun.* **1973**, *13*, 435.
(41) Leslie, F. M. *J. Phys. D* **1976**, *9*, 925.
(42) Leslie, F. M. *Adv. Liq. Cryst.* **1979**, *4*, 1.
(43) Archer, L. A.; Larson, R. G. *J. Chem. Phys.* **1995**, *103*, 3108.
(44) Subbotin, A. *Macromolecules* **1993**, *26*, 2562.
(45) Greco, F.; Marrucci, G. *Mol. Cryst. Liq. Cryst.* **1997**, *22*, 11.
(46) Huang, C. M.; Magda, J. J.; Larson, R. G. *J. Rheol.* **1999**, *43*, 31.
(47) Andresen, E. M.; Mitchell, G. R. *Europhys. Lett.* **1998**, *43*, 296.
(48) Pieranski, P.; Guyon, E. *Phys. Rev. A* **1974**, *9*, 404.

MA0018493